Evaluation of Detection Performance under Employment of the Generalized Detector in Radar Sensor Systems

Modar SHBAT, Vyacheslav TUZLUKOV

School of Electronics Engineering, College of IT Engineering, Kyungpook National University,
1370 Sankyuk-dong, Bug-gu, Daegu, South Korea

modboss80@knu.ac.kr, tuzlukov@ee.knu.ac.kr

Abstract. *The detection performance of the generalized detector (GD) constructed based on the generalized approach to signal processing in noise is evaluated under homogeneous and non-homogeneous noise. The GD adaptive threshold is derived and defined applying an appropriate noise power estimation using the sliding window technique. The direct close expressions for the GD average probability of detection and probability of false alarm are also derived. Typical constant false alarm rate (CFAR) detectors, namely, the cell averaging CFAR (CA-CFAR) detector, the ordered statistic CFAR (OS-CFAR) detector, the generalized censored mean level (GCML) detector, and the adaptive censored greatest-of CFAR (ACGO-CFAR) detector are compared with the GD by detection performance under both homogeneous and non-homogeneous noise conditions, i.e. when the interfering targets are absent or present, respectively. Simulation results demonstrate a superiority of GD in detection performance in comparison with the above mentioned CFAR detectors under both homogeneous and non-homogeneous noise conditions.*

Keywords

Constant false alarm rate (CFAR) detector, generalized detector (GD), homogeneous noise, non-homogeneous noise, signal-to-noise ratio (SNR), detection performance, adaptive detection threshold.

1. Introduction

Employing any radar sensor system we are interested to solve the following problem: a presence or absence of the target return signal that is always embedded in noise or, in another words, a "yes" or a "no" target. Additionally, we are interested to extract any information about the target parameters, for example, the target range, relative velocity, azimuth angle, elevation angle, and others. Quality of detector performance is defined by the probability density function (pdf) of observed data samples [1, Chapter 6, pp. 312-319]. The decision making strategy leads us to a definition of detection threshold. As a rule, the detection threshold is defined based on the fixed probability of false alarm and estimated noise power or noise variance [2]. Ability to detect the target return signal is limited by presence of noise and interference or clutter that are the stochastic processes by nature. In practice, the noise and interference power are variable. The constant false alarm rate (CFAR) detectors are designed in order to provide predictable detection and false alarm rate statistics in realistic scenario [1, Chapter 7, pp. 347-382].

Noise power estimation techniques are widely used in signal processing systems, communication systems, cognitive radio, speech recognition, radar sensor, remote sensing, and others. Appropriate noise power estimation procedure is needed to define the adaptive detection threshold and should provide a required balance between the small estimation error and effective tracking ability in the case of non-stationary noise [3]. The CFAR detectors are widely used by radar sensor systems in many applications. For instance, the middle range and short range radar sensors are implemented in vehicle safety driving technologies [4]-[9]. In the case of CFAR detector implementation, the noise power can be estimated after processing the observed data stored in the specified number of reference cells using the sliding window technique. The required adaptive detection threshold is defined as a product between the estimated noise power and the scaling factor, see [10] and [11]. Detectors constructed based on this principle are differed by processing procedures of data stored in the reference cells of sliding window. Cell averaging CFAR (CA-CFAR) detector has an optimum detection performance in the case of homogeneous noise. CA-CFAR detector estimates the noise power by averaging a power of observed data stored in the reference cells of sliding window. The adaptive detection threshold is defined after noise power estimation [10].

In many practical cases, there is the non-homogeneous noise according to spatial and temporal variations in the noise power and closely spaced target return signals that may be a reason of the estimated noise power bias and, consequently, the detection threshold is varied [12], [13]. The ordered statistics CFAR (OS-CFAR) detector is implemented in the case of non-homogeneous noise and multiple targets [11], [14]. OS-CFAR detector rearranges the reference cell data in ascending numerical order with the purpose to form a new data sequence where the *k*th order

statistic is selected as the noise power. Almost all detectors are employed under non-homogeneous noise conditions, for example, the generalized censored mean level (GCML) detector and the adaptive censored greatest-of CFAR (ACGO-CFAR) detector discussed in [15], [16], respectively. The GCML detector discards the data associated with interfering targets in the reference cells of the sliding window (censoring process) before definition of the noise power and detection threshold. ACGO-CFAR detector reduces the clutter edge false alarm effects when the test cell is close to the boundary between two interference regions. ACGO-CFAR detector defines the average noise power in the leading and lagging windows (the reference window is divided on two subwindows where the test cell is in the middle between them) separately after using the censoring process. The required estimated noise power is selected as the maximal averaged value.

The generalized detector (GD) constructed based on the generalized approach to signal processing in noise [17] is a combination of the correlation detector that is optimal in the Neyman-Pearson (NP) criterion sense under detection of signals with known parameters, and the energy detector, which is optimal in the NP criterion sense under detection of signals with unknown parameters. This combination allows us to formulate a decision-making rule based on definition of the jointly sufficient statistics of the mean and variance of the likelihood function [18]. There is a need to note that a decision-making rule for the correlation detector is made based on definition of the sufficient statistics of the likelihood function mean only, while for the energy detector a decision-making rule is made based on definition of the sufficient statistics of the likelihood function variance only. Using the generalized approach to signal processing in noise, we obtain additional information in the form of the jointly sufficient statistics of the likelihood function variance and mean in comparison with the correlation and energy detectors, respectively. The GD implementation in radar sensor systems is discussed in [19]-[21] in the case of the linear frequency modulation continuous wave radar sensor system for short and middle range radar applications such as the closing vehicle detection and blind spot detection in automotive safety driving applications [22].

In this paper, we employ two noise power estimation techniques based on the sliding window procedure of a specified number of reference cells. In the case of homogeneous noise, the noise power is estimated by averaging the observed data stored in the reference cells of sliding window. In the case of non-homogenous noise and multiple targets, the procedure of ordered statistics is applied to the observed data stored in the reference cells of sliding window with the purpose to estimate the noise power. This technique is also used by the OS-CFAR detector and demonstrates the better performance for the multitarget environment in comparison with the mean level CFAR detector family including the CA-CFAR, greatest of CFAR (GO-CFAR), and smallest of CFAR (SO-CFAR). Several CFAR detectors employed by radar sensor system under homogeneous and non-homogeneous are evaluated in [23].

Comparative analysis of detection performances between GD and various CFAR detectors, namely, CA-CFAR, OS-CFAR, GCML, and ACGO-CFAR under both homogeneous and non-homogeneous noise is made at the same initial conditions. The simulation results demonstrate a superiority of the GD in detection performance over the mentioned above CFAR detectors in the case of both homogeneous and non-homogeneous noise.

The rest of this paper is organized as follows. A brief review of discussed CFAR detectors is introduced in Section 2. The basic GD structure and definition of the adaptive detection threshold and the probability of detection for radar sensor systems are discussed in Section 3. Section 4 presents the noise power estimation procedure based on the sliding window technique for GD. The simulation results are discussed in Section 5. Finally, the conclusion remarks are presented in Section 6.

2. CFAR Detectors

The fixed probability of false alarm P_{FA} is a desirable requirement for radar sensor systems, especially, in the case of high duty cycle owing to the noise sensitivity reason. There is a need to define the adaptive detection threshold based on the noise power estimation. For any CFAR detector, the noise power is estimated by processing the data stored in the reference cells of sliding window. We discuss briefly several CFAR detectors, namely, CA-CFAR, OS-CFAR, GCML, and ACGO-CFAR detectors.

2.1 CA-CFAR Detector

The CA-CFAR detector has an optimum detection performance among the mean level CFAR detector family in the case of homogeneous noise when the neighboring reference cells of sliding window contain the noise data obeying the same pdf and having the same statistical parameters as the data stored in the test cell of sliding window [10]. CA-CFAR detector estimates the noise power by averaging the data in the reference cells of sliding window. The adaptive detection threshold is defined based on this procedure. Basic CA-CFAR detector functioning principle is shown in Fig. 1. The estimated noise power Z_{CA} is determined in the following from:

$$Z_{CA} = \frac{1}{N} \sum_{j=1}^{N} X_j \ , \tag{1}$$

where X_j are the energy detector output samples stored by the reference cells, and N is the number of reference cells of sliding window. In this case, the probability of detection P_D can be determined in the following form [10]:

$$P_D^{CA} = \left(1 + \frac{\alpha_{CA}}{N(1+SNR)}\right)^{-N}, \tag{2}$$

where SNR is the average signal-to-noise ratio and α_{CA} is the scaling factor for CA-CFAR detector given as a func-

tion of the reference cell number N and the probability of false alarm P_{FA}

$$\alpha_{CA} = N[(P_{FA})^{-1/N} - 1] \;.\tag{3}$$

The adaptive CA-CFAR detection threshold can be presented in the following form [10]:

$$THR_{CA} = \alpha_{CA} Z_{CA} \;.\tag{4}$$
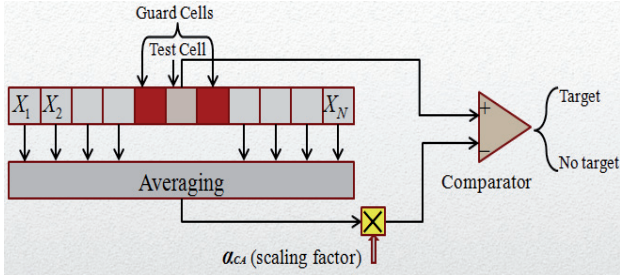
Fig. 1. Functioning principle of CA-CFAR detector.

2.2 OS-CFAR Detector

In practice, the non-homogeneous noise is caused by both spatial and temporal variations in the noise power and, additionally, by the closely spaced target return signals that is a reason of the estimated noise power bias and, consequently, the detection threshold variations. As a rule, the OS-CFAR detector is employed under the non-homogeneous noise conditions [11]. In the multitarget case, the detection performance of OS-CFAR detector is much better than the detection performance of the mean level CFAR detector family [3], including the CA-CFAR detector, greatest-of CFAR (GO-CFAR) detector, and smallest-of CFAR (SO-CFAR) detector. OS-CFAR detector rearranges the data samples $\{X_1,…,X_N\}$ in the reference cells of sliding window to form a new sequence of data samples $\{X_{(1)} \le X_{(2)} \le … \le X_{(k)} \le …\le X_{(N)}\}$ according to the increasing order, where the $X_{(k)}$ element of the ordered data samples is called the kth order statistics assigned as the noise power (Fig. 2). This approach is based on the fact that the interfering signal power is usually higher than the noise power. The minimal loss in SNR for OS-CFAR detector is achieved when the order of statistic k is given as [11]

$$k = \frac{3}{4} N \;.\tag{5}$$

The OS-CFAR detector is able to reject the number of interfering targets equal to $N - k$. The probability of detec
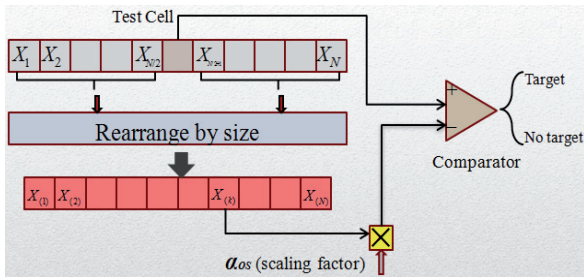
Fig. 2. Functioning principle of OS-CFAR detector.

tion P_D for OS-CFAR detector is determined by the following form [11]:

$$P_D^{OS} = \prod_{j=0}^{k-1} \frac{N - j}{N - j + \dfrac{\alpha_{OS}}{1 + SNR}} \;.\tag{6}$$

The scaling factor α_{OS} takes the following form [11]:

$$\alpha_{OS} = (P_{FA})^{-1/k} - 1 \;.\tag{7}$$

Finally, the adaptive OS-CFAR detection threshold can be determined in the following form:

$$THR_{OS} = \alpha_{OS} X_{(k)} \;.\tag{8}$$

2.3 GCML Detector

GCML detector is also employed under the non-homogeneous noise [15]. The GCML detector (see Fig. 3) can cancel the interfering target data stored in the reference cells of sliding window prior to noise power definition using the censoring process. There is no need to know a priori the number of interfering targets as in the case of OS-CFAR detector. The sliding window is divided on two windows equal by length: the leading window $\{X_1, X_2,…,X_M\}$ when $M = N/2$, and the lagging window $\{X_{M+1}, X_{M+2}, …,X_{2M}\}$. The reference cell data of these two windows are processed independently in parallel way by the censoring processes.

The censoring algorithm ranks the reference cell data of these two windows in ascending numerical order like $\{X_{(1)} \le … \le X_{(M)}\}$ and $\{X_{(M+1)} \le X_{(M+2)} \le …\le X_{(2M)}\}$., respectively. The algorithm assigns the lowest order $X_{(1)}$ as the noise power reading and defines the threshold $THR_{X_{(1)}} = \alpha_1 X_{(1)}$, where α_n, in a general case, is the scaling factor chosen to achieve the required probability of false censoring P_{FC}, and $n = 1,.., M - 1$. The probability of false censoring P_{FC} can be determined in the following form [15]:

$$P_{FC} = \frac{(M - n + 1)}{(1 + \alpha_{M-n})^{M-n}} \;.\tag{9}$$

The threshold $THR_{X_{(1)}}$ is compared with the reading $X_{(2)}$. If the reading $X_{(2)}$ is greater than the threshold $THR_{X_{(1)}}$, the data $\{X_2, X_3,...,X_M\}$ are considered as the result of energy detector processing of the interfering target signals. If the following condition $X_{(2)} < THR_{X_{(1)}}$ is satisfied we can make a decision that $X_{(2)}$ is the noise sample without interference. After that the censoring algorithm forms the sum of two lower ordered samples $X_{(1,2)} = X_{(1)} + X_{(2)}$, defines the threshold $THR_{X_{(1,2)}}$ and compares the threshold $THR_{X_{(1,2)}}$ with the reading $X_{(3)}$. The censoring process is stopped if a decision "a yes" signal is made. More discussion about GCML detector can be found in [15].
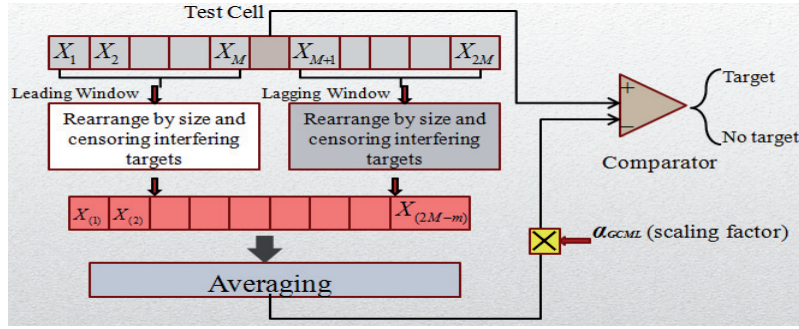
Fig. 3. Functioning principle of GCML detector.
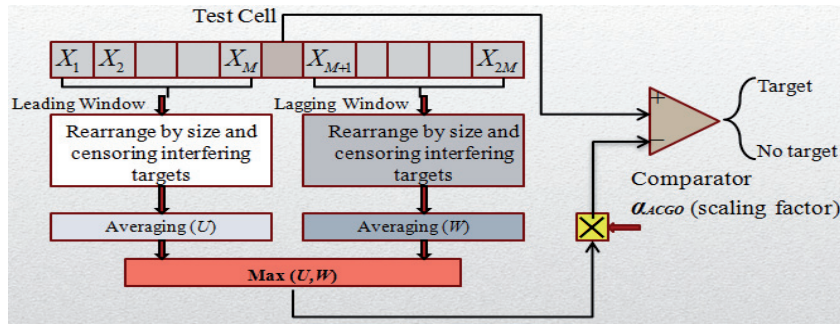
Fig. 4. Functioning principle of ACGO-CFAR detector.

2.4 ACGO-CFAR Detector

The ACGO-CFAR detector can be considered as a modified version of the GCML detector in order to reduce the clutter edge false alarm, when the test cell is close to the boundary between two interference regions. The statistics in the leading and lagging windows will not be the same [16]. The ACGO-CFAR detector suppresses the clutter edge false alarm by definition of the average noise power in the leading and lagging windows individually and selects the highest averaged noise power value to consider it as the required estimated noise power. The functioning principle of ACGO-CFAR detector is presented in Fig. 4. We assume that n_1 samples are censored from the leading window cells and n_2 samples are censored from the lagging window cells. The remaining samples from the leading window $m_1 = M - n_1$ and from the lagging window $m_2 = M - n_2$, where $M = N/2$, are used to estimate the noise power as follows [16]:

$$U = \frac{1}{m_1} \sum_{j=1}^{m_1} X_{(j)} \, , \qquad W = \frac{1}{m_2} \sum_{j=1}^{m_2} X_{(j)} \, . \qquad (10)$$

The estimated noise power is set to be the maximum of U and W [16]:

$$Z_{ACGO} = \max(U, W) \, . \qquad (11)$$

3. GD Main Functioning Principles. Definition of Detection Threshold

3.1 GD Functioning Principles and Structure

Simple GD flowchart is represented in Fig. 5. For this block diagram we use the following notations: MSG is the model signal generator (the local oscillator), AF is the additional filter (the linear system), and PF is the preliminary filter (the linear system). A detailed discussion of the AF and PF can be found in [17], [18, Chapter 3].

Consider briefly the main statements regarding the AF and PF. There are two linear systems at the GD front end that can be considered, for example, as the bandpass filters, namely, the PF with the impulse response $h_{PF}(\tau)$ and the AF with the impulse response $h_{AF}(\tau)$. For simplicity of analysis, we think that AF and PF have the same amplitude-frequency responses by shape and bandwidths by value. Moreover, a resonant frequency or central frequency of the AF is detuned relative to a resonant frequency or central frequency of the PF on such a value that the target return signal cannot pass through the AF, i.e. on a value exceeding the target return signal bandwidth. Thus, the target return signal plus noise can be appeared at the PF output and only the reference noise is appeared at the AF output.
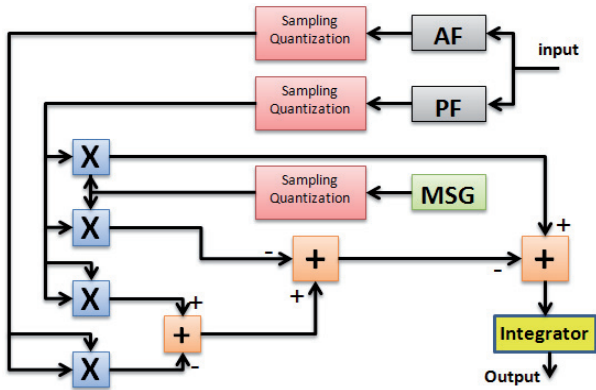
Fig. 5. Principal flowchart of GD.

It is well known [17], if a value of detuning between the AF and PF resonant or central frequencies is more than 4 to 5 times the target return signal bandwidth Δf, the processes forming at the AF and PF outputs can be considered as independent and uncorrelated. In practice, the coefficient of correlation is not more than 0.05 that was confirmed experimentally in [24], [25]. In the case of a "no" target return signal in the input stochastic process, the statistical parameters at the AF and PF outputs will be the same, because the same noise is coming in at the AF and PF inputs, and we may think that the AF and PF do not change the statistical parameters of input process since they are the linear GD front end systems. By this reason, the AF can be considered as a generator of reference noise sample with a priori information a "no" target return signal.

There is a need to make some comments regarding the noise forming at the PF and AF outputs. If the additive white Gaussian noise (AWGN) $w(t)$ with zero mean and two-sided power spectral density $0.5\mathcal{N}_0$ comes in at the AF and PF inputs (the GD linear system front end), the noise forming at the AF and PF outputs is the narrowband Gaussian process with zero mean and variance determined as [18, Chapter 3]

$$\sigma_n^2 = \frac{\mathcal{N}_0 \omega_0^2}{8\Delta_F} \quad , \tag{12}$$

where, in the case if, for example, AF or PF is the RLC oscillatory circuit, the AF or PF bandwidth Δ_F and resonance frequency ω_0 are defined in the following manner $\Delta_F = \pi\beta$, $\omega_0 = \dfrac{R}{\sqrt{LC}}$, $\beta = \dfrac{R}{2L}$, because the AF and PF are the linear systems.

In a general case, the narrowband Gaussian noise forming at the PF and AF outputs take the following form[17]:

$$\begin{cases} w_{PF}(t) = \zeta(t) = \displaystyle\int_{-\infty}^{\infty} h_{PF}(\tau)w(t-\tau)d\tau \ ; \\ w_{AF}(t) = \eta(t) = \displaystyle\int_{-\infty}^{\infty} h_{AF}(\tau)w(t-\tau)d\tau \ . \end{cases} \tag{13}$$

The main functioning condition of GD is an equality over the whole range of parameters between the model signal forming at the GD MSG output (the searching signal) and the detected target return signal coming in at the GD input linear system (the PF) output. How we can satisfy this condition in practice is discussed in detail in [17], [18, Chapter 7]. More detailed discussion about a choice of PF and AF and their impulse responses is given in [26, Chapter 5], [27, Chapter 2].

Assume S_i is the sample of input stochastic process, a_i is the target return signal, w_i is the additive white Gaussian noise with zero mean and variance σ_n^2, $i = 1,\dots, K$. The simplest signal detection problem can be presented in the following form:

$$S_i = \begin{cases} a_i + w_i, \ i = 1,...,K \ \Rightarrow \mathcal{H}_1 \\ w_i, \qquad i = 1,...,K \ \Rightarrow \mathcal{H}_0 \end{cases}, \tag{14}$$

where K is the sample size; $\mathcal{H}_1$ is the hypothesis a "yes" signal; and $\mathcal{H}_0$ is the alternative hypothesis. If the probability of false alarm P_{FA} is fixed, we can apply the Neyman-Pear-son criterion, for which the probability of detection P_D is maximal for any signal-to-noise ratio (SNR).

In practice, in order to maintain permanently a physical sense of signal detection, we should distinguish the target return signal a_i and its model a_i^{mod} forming at the GD MSG output. In radar sensor systems, the model signal a_i^{mod} is considered as the searching signal generated by the GD MSG. The model signal can be presented in the following form:

$$a_i^{\text{mod}} = \mu \, a_i \quad , \tag{15}$$

where μ is the coefficient of proportionality.

Implementation of the generalized approach to signal processing in noise assumes modifications concerning the initial premises of classical and modern signal detection theories [17], [18, Chapter 3]. In accordance with the generalized approach to signal processing in noise, the signal detection algorithm can be presented in the following form:

$$\sum_{i=1}^{K} 2Y_i a_i^{\text{mod}} - \sum_{i=1}^{K} Y_i^2 + \sum_{i=1}^{K} \eta_i^2 \overset{\mathcal{H}_1}{\underset{\mathcal{H}_0}{\gtrless}} THR_{GD} \ , \tag{16}$$

where Y_i is the sample of observed stochastic process at the PF output, η_i is the sample of observed noise at the AF output, and THR_{GD} is the GD threshold. The first term in (16) corresponds to the correlation detector with twice the gain and is considered as the sufficient statistics of the likelihood function mean. The second term in (16) corresponds to the energy detector and is considered as the sufficient statistics of the likelihood function variance [17], [18, Chapter 3].The third term in (16) presents the reference noise power generated according to the main functioning principles of the generalized approach to signal processing in noise. Equation (16) represents the decision-making rule
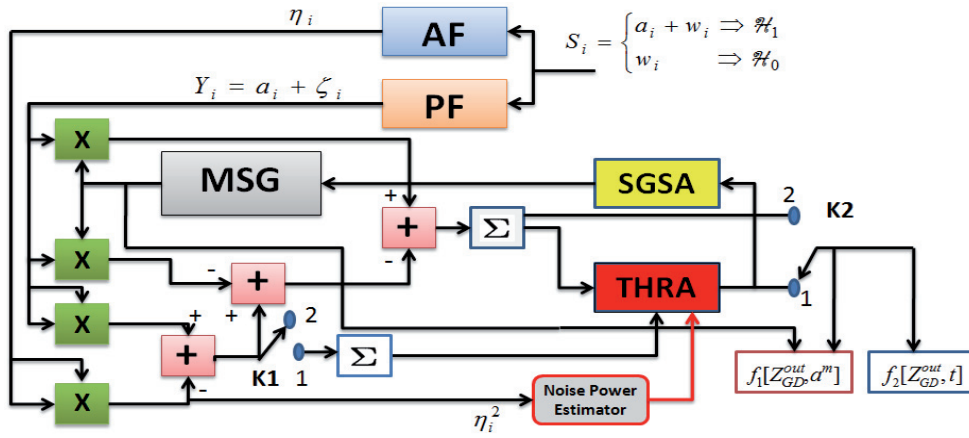
Fig. 6. Practical GD flowchart.

under the implementation of the generalized approach to signal processing in noise for any signal processing system.

For practical purposes, we can use the GD flowchart presented in Fig. 6, in which the threshold apparatus (THRA) device defines the GD threshold, and the signal model generator switching apparatus (SGSA) is used to switch on the MSG to define the unknown parameters of the detected target return signal. The switch K1 takes the position "1" to define the GD threshold THR_{GD} and takes the position "2" after the GD threshold definition and the target return signal detection has been carried out. The switch K2 is used to put the THRA device in and out of service.
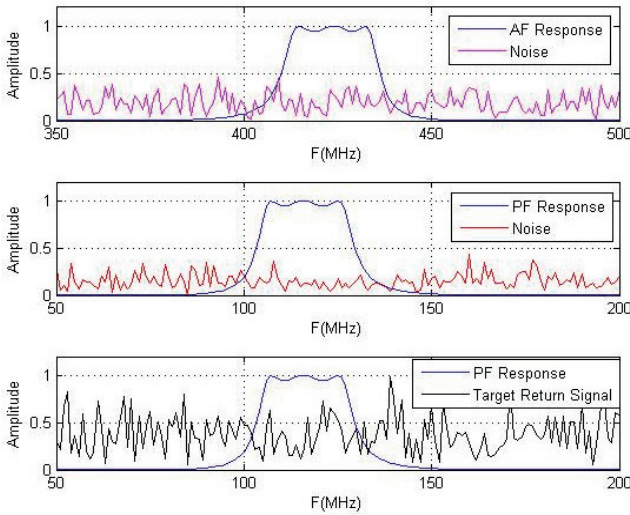
Fig. 7. The signals at the AF and PF outputs.

In the case of a "yes" target return signal (the hypothesis $\mathcal{H}_1$), when $Y_i = a_i + \zeta_i$, where ζ_i is the sample of the observed narrowband noise at the PF output, the left side in (16) takes a form: $\sum_{i=1}^{K} a_i a_i^{\mathrm{mod}} + \sum_{i=1}^{K} \eta_i^2 - \sum_{i=1}^{K} \zeta_i^2$, where the first term can be considered as the signal energy if the condition $a_i^{\mathrm{mod}} = a_i$ is satisfied, and a linear combination of the second and third terms $\sum_{i=1}^{K} \eta_i^2 - \sum_{i=1}^{K} \zeta_i^2$ represents the background noise at the GD output.

The background noise is a difference between the narrowband noise power forming at the PF and AF outputs. In the opposite case, i.e. a "no" target return signal (the hypothesis $\mathcal{H}_0$), when $Y_i = \zeta_i$, the left side in (16) is the background noise $\sum_{i=1}^{K} \eta_i^2 - \sum_{i=1}^{K} \zeta_i^2$ only if the condition $a_i^m = a_i$ is satisfied. Thus, the target return signal a_i and the narrowband noise ζ_i can be appeared at the PF output and the narrowband noise η_i is appeared at the AF output only (see Fig. 7). In (16), the second term corresponds to the energy detector incorporated in the GD and coupled with the PF.

3.2 GD Detection Threshold

We assume that the noise forming at the PF and AF outputs is the narrowband process with the Rayleigh amplitude envelope and the phase uniformly distributed within the limits of the interval $[0, 2\pi)$. In this case, the GD background noise pdf takes the following form [18]:

$$p_{Z_{GD}^{\mathcal{H}_0}}(z) = \begin{cases} \dfrac{1}{2\sigma_n^2} \exp\left(-\dfrac{|z|}{2\sigma_n^2}\right), & z \geq 0 \\ 0 & z < 0 . \end{cases} \tag{17}$$

As we can see from (17), the pdf of the background noise forming at the GD output under the hypothesis $\mathcal{H}_0$ is defined by the exponential type distribution when the time interval $[0, T]$ is infinitesimal $(T \to 0)$ [18, Chapter 3]. Based on (17), the probability of false alarm P_{FA} can be presented in the following form:

$$P_{FA}^{GD} = \int_{THR_{GD}}^{\infty} p_{Z_{GD}^{\mathcal{H}_0}}(z)dz = \exp\left(-\frac{THR_{GD}}{2\sigma_n^2}\right). \tag{18}$$

According to (18), the GD threshold can be determined in terms of P_{FA} using the following equation:

$$THR_{GD} = -2\sigma_n^2 \ln(P_{FA}^{GD}). \tag{19}$$

If the scaling factor

$$\gamma_{GD} = -2\ln(P_{FA}^{GD}) \qquad (20)$$

is applied, the modified adaptive GD threshold takes the following form:

$$THR_{GD} = \sigma_n^2 \gamma_{GD} . \qquad (21)$$

Taking (20) into consideration, the probability of false alarm P_{FA} can be presented in the following form:

$$P_{FA}^{GD} = \exp(-0.5\gamma_{GD}) . \qquad (22)$$

The last equation allows us to determine the probability of false alarm P_{FA}^{GD} for a given scaling factor γ_{GD} or to determine the required scaling factor γ_{GD} for the fixed probability of false alarm P_{FA}^{GD}.

3.3 GD Detection Performance

Now consider the hypothesis $\mathcal{H}_1$ when the fluctuating target return signal is presented. The pdf of the background noise at the GD output given in (17) obeys the exponential type law. Based on (17), the pdf of the decision statistics forming at the GD output under the hypothesis $\mathcal{H}_1$ can be presented in the following form:

$$p_{Z_{GD}^{\mathcal{H}_1}}(z) = \frac{1}{2(\sigma_n^2 + \sigma_s^2)} \exp\left(-\frac{z}{2(\sigma_n^2 + \sigma_s^2)}\right), \qquad (23)$$

where σ_s^2 is the variance of the fluctuating target return signal modeled as Swerling 2 model. The probability of detection P_D^{GD} can be presented in the following form:

$$P_D^{GD} = \int_{THR_{GD}}^{\infty} p_{Z_{GD}^{\mathcal{H}_1}}(z)dz$$

$$= \int_{THR_{GD}}^{\infty} \frac{1}{2(\sigma_n^2 + \sigma_s^2)} \exp\left(-\frac{z}{2(\sigma_n^2 + \sigma_s^2)}\right)dz . \qquad (24)$$

Introducing the signal-to-noise ratio $SNR = \sigma_s^2/\sigma_n^2$, we can rewrite the probability of detection P_D as

$$P_D^{GD} = \int_{THR_{GD}}^{\infty} \frac{1}{2\sigma_n^2(1+SNR)} \exp\left(-\frac{z}{2\sigma_n^2(1+SNR)}\right)dz . \quad (25)$$

After some mathematical transformations and calculation of the integral in (25), the probability of detection P_D^{GD} takes the following form:

$$P_D^{GD} = \exp\left(-\frac{THR_{GD}}{2\sigma_n^2(1+SNR)}\right) . \qquad (26)$$

Taking into consideration the detection threshold THR_{GD} given in (19), the probability of detection P_D^{GD} can be rewritten as

$$P_D^{GD} = \exp\left(\frac{\ln(P_{FA}^{GD})}{1+SNR}\right) . \qquad (27)$$

4. GD Noise Power Estimation Techniques

The GD threshold is continuously updated based on the noise variance variations at the GD AF output under non-homogeneous noise conditions at the GD input (the adaptive GD threshold). Thus, there is a need to apply the noise power estimation technique in order to define the adaptive GD threshold. If the noise at the GD input is Gaussian, the narrowband noise forming at the GD AF and PF outputs is Gaussian too with the same variance σ_n^2, because AF and PF are the linear systems. Owing to the fact that the frequency content of interfering signals is within the limits of GD PF bandwidth, the noise power estimation is not affected by these interfering signals because the noise reference samples forming at the AF GD output are used under employment of the required estimation procedure. In the case when the frequency content of interference caused, for example, by jammer or any other sources, is within the limits of GD AF bandwidth, the background noise power estimation procedure will be affected.

Two narrowband noise power estimation procedures are applied based on the sliding window technique. The first narrowband noise power estimation procedure is based on averaging the data stored in the reference cells of sliding window (Fig. 8a). The second narrowband noise power estimation procedure is carried out by ordered statistic processing as in the case of OS-CAFR detector (Fig. 8b).
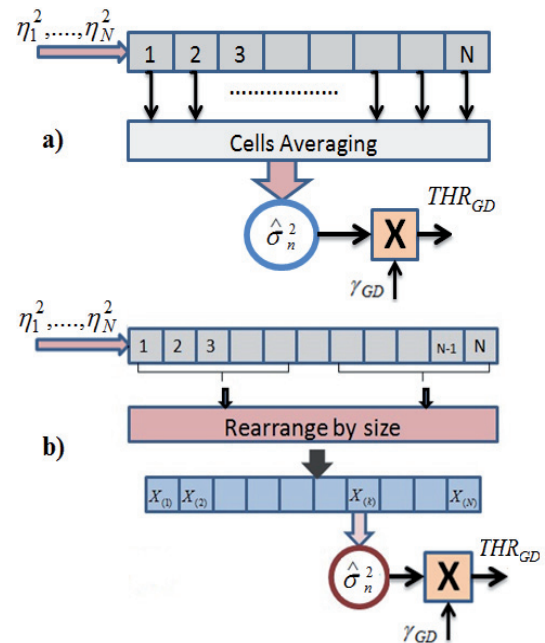
Fig. 8. GD noise power estimation techniques: a) cell averaging technique, b) ordered statistic technique.

4.1 Cell Averaging Technique

The estimation of the narrowband noise power is performed under assumption of independent and identically distributed (i.i.d) narrowband noise data stored in the refer-
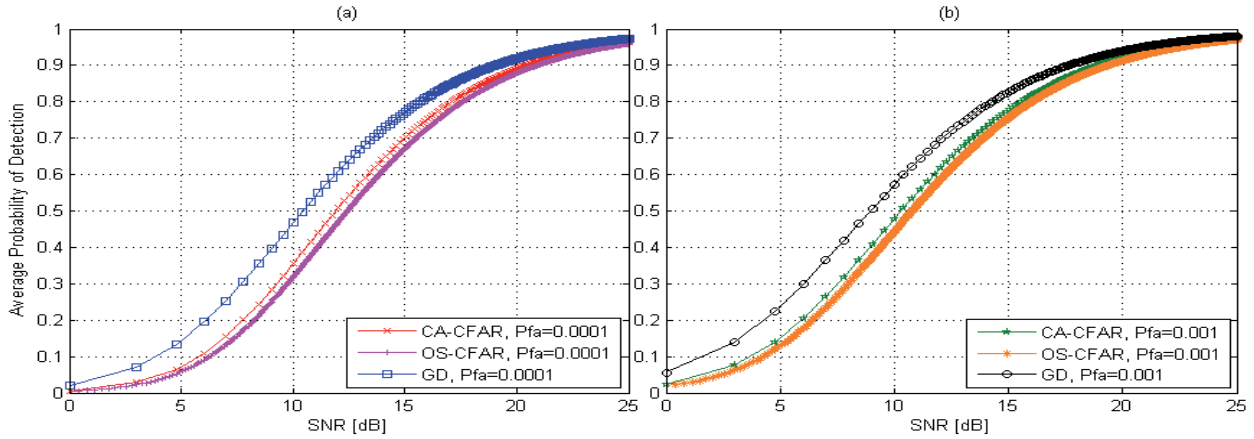
Fig. 9. Theoretical average detection performance for GD, CA-CFAR, and OS-CFAR detectors: a) $P_{FA} = 0.0001$, b) $P_{FA} = 0.001$.

ence cells of the sliding window. The estimated narrow-band noise power in the course of reference cell data averaging procedure can be presented by processing the noise sample $\eta_1, \dots, \eta_N$ forming at the GD AF output:

$$\hat{\sigma}_n^2 = \frac{1}{N} \sum_{i=1}^{N} \eta_i^2 . \qquad (28)$$

Taking (19) into consideration, the adaptive GD detection threshold after narrowband noise power estimation can be determined as

$$THR_{GD} = -2\hat{\sigma}_n^2 \ln(P_{FA}^{GD}) . \qquad (29)$$

The definition of the GD average probability of detection $\overline{P_D^{GD}}$ helps us to find a relationship between the GD detection performance and the number of reference cells in the sliding window N. The GD average probability of detection $\overline{P_D^{GD}}$ can be presented in the following form:

$$\overline{P_D^{GD}} = \int_{-\infty}^{\infty} P_D^{GD} p_{CA}(THR_{GD}) d(THR_{GD}) , \qquad (30)$$

where $p_{CA}(THR_{GD})$ is the GD threshold pdf in the case of cell-averaged noise power estimation technique that can be defined in the following form based on the procedure discussed in [1]

$$p_{CA}(THR_{GD}) = \left(\frac{N}{\gamma_{GD}\sigma_n^2}\right)^N \frac{THR_{GD}^{N-1}}{(N-1)!} \exp\left(-N\frac{THR_{GD}}{\gamma_{GD}\sigma_n^2}\right) . \qquad (31)$$

Based on (30) and (31), the average probability of detection $\overline{P_D^{GD}}$ is determined as

$$\overline{P_D^{GD}} = \int_{-\infty}^{\infty} \left(\frac{N}{\gamma_{GD}\sigma_n^2}\right)^N \frac{THR_{GD}^{N-1}}{(N-1)!}$$

$$\times \exp\left(-\frac{THR_{GD}}{2\gamma_{GD}\sigma_n^2} \times \frac{2N(1+SNR)+\gamma_{GD}}{1+SNR}\right) d(THR_{GD}). \qquad (32)$$

Using the tabulated integral [28]

$$\int_0^\infty x^b \exp(-ax) = \frac{b!}{a^{b+1}} , \quad a > 0, \quad b = 0, 1, 2, \dots \qquad (33)$$

we can find that the average probability of detection $\overline{P_D^{GD}}$ is determined in the following form:

$$\overline{P_D^{GD}} = \left(1 + \frac{\gamma_{GD}}{2N(1+SNR)}\right)^{-N} . \qquad (34)$$

The theoretical detection performance of the GD, CA-CFAR, and OS-CFAR detectors is presented in Fig. 9 based on (2), (6), and (34) at $P_{FA} = 10^{-3}$ and $P_{FA} = 10^{-4}$. Comparison shows the GD superiority over the CA-CFAR and OS-CFAR detectors. For example, at $P_{FA} = 10^{-4}$, the GD runs up approximately 2 dB SNR gain in comparison with CA-CFAR detector and 2.5 dB SNR gain in comparison with OS-CFAR detector at the probability of detection P_D equal to 0.6. The theoretical detection performance of the GCML detector is almost identical with the CA-CFAR detector under homogeneous noise conditions.

Any detector will be considered as a CFAR detector if the averaged value of the probability of false alarm is independent of the actual value of noise power. In the case of GD, the average value of P_{FA}^{GD} is defined as

$$\overline{P_{FA}^{GD}} = \int_{-\infty}^{+\infty} \exp\left(-\frac{THR_{GD}}{2\sigma_n^2}\right) p_{CA}(THR_{GD}) d(THR_{GD})$$

$$= \int_{-\infty}^{+\infty} \left(\frac{N}{\gamma_{GD}\sigma_n^2}\right)^N \frac{THR_{GD}^{N-1}}{(N-1)!} \exp\left(-\frac{THR_{GD}(2N+\gamma_{GD})}{2\gamma_{GD}\sigma_n^2}\right) d(THR_{GD}). \qquad (35)$$

Taking (33) into consideration, we obtain from (35):

$$\overline{P_{FA}^{GD}} = \left(1 + \frac{\gamma_{GD}}{2N}\right)^{-N} . \qquad (36)$$

As we can see from (36), the average GD probability of false alarm $\overline{P_{FA}^{GD}}$ does not depend on the actual noise power σ_n^2. Thus, the GD keeps the CFAR property.

In practice, the observed GD probability of false alarm $P_{FA_{ob}}^{GD}$ is not exactly the desired value. Let $P_{FA_{des}}^{GD}$ be the desired GD probability of false alarm when the estimated noise power is equal to $\hat{\sigma}_n^2$. In this case, the GD threshold is given as $\widehat{THR}_{GD} = -2\hat{\sigma}_n^2 \ln(P_{FA_{des}}^{GD})$. Taking (18) into consideration, we can determine the observed GD probability of false alarm $P_{FA_{ob}}^{GD}$ using the following form:

$$
P_{FA_{ob}}^{GD} = \exp\left\{\frac{2\hat{\sigma}_n^2 \ln(P_{FA_{des}}^{GD})}{2\sigma_n^2}\right\}
$$

$$
= \exp\left\{\ln\left\{\left[P_{FA_{des}}^{GD}\right]^{\frac{\hat{\sigma}_n^2}{\sigma_n^2}}\right\}\right\} = \left[P_{FA_{des}}^{GD}\right]^{\frac{\hat{\sigma}_n^2}{\sigma_n^2}}. \tag{37}
$$

Based on (37) we can find that the desired and observed probabilities of false alarm will be the same if the real and estimated noise powers are the same.

A relatively simple estimate that can approximate the effect of interfering target which has frequency content matched with the AF bandwidth can be derived. Let us consider a single interfering target with power I_i that is existed only in one reference cell of the sliding window. The interference-to-noise ratio (*INR*) or the SNR of this interferer is $INR = I_i/\sigma_n^2$. The expected value of the new GD threshold given by

$$
\widehat{THR}_{GD} = \frac{\gamma_{GD}}{N}\left(I_i + \sum_{i=1}^{N-1}\eta_i^2\right) \tag{38}
$$

can be presented in the following form:

$$
\mathrm{E}\left[\widehat{THR}_{GD}\right] = \mathrm{E}\left[\frac{\gamma_{GD}}{N}\left(I_i + \sum_{i=1}^{N-1}\eta_i^2\right)\right] = \frac{\gamma_{GD}I_i}{N} + \gamma_{GD}\hat{\sigma}_n^2
$$

$$
= \gamma_{GD}\left(1 + \frac{INR}{N}\right)\hat{\sigma}_n^2. \tag{39}
$$

The GD scaling factor in the case when the cell averaging noise power estimation technique is used can be easily defined based on (36) as

$$
\gamma_{GD} = 2N\left[\left(\overline{P_{FA}^{GD}}\right)^{-1/N} - 1\right]. \tag{40}
$$

As follows from (39), the expected value of the new threshold is a multiple of the estimated noise power with a new multiplier (scaling factor) given by

$$
\widetilde{\gamma}_{GD} = \gamma_{GD}\left(1 + \frac{INR}{N}\right). \tag{41}
$$

The new GD threshold with the existence of the interfering target will decreases both the probability of detection and the probability of false alarm. Using (34), (39), and (41) we can find the expression for the new average probability of detection:

$$
\overline{\widetilde{P}_D^{GD}} = \left(1 + \frac{\widetilde{\gamma}_{GD}}{2N(1 + SNR)}\right)^{-N}
$$

$$
= \left\{1 + \frac{2N\left[\left(\overline{P_{FA}^{GD}}\right)^{-1/N} - 1\right]\left[1 + \frac{INR}{N}\right]}{2N(1 + SNR)}\right\}^{-N}
$$

$$
= \left\{1 + \left[\left(\overline{P_{FA}^{GD}}\right)^{-1/N} - 1\right] \times \frac{N + INR}{N(1 + SNR)}\right\}^{-N}. \tag{42}
$$

We can see from (42) as $INR \to 0$ (no interfering target) or $N \to \infty$ when the interfering target influence becomes very small or negligible, $\overline{\widetilde{P}_D^{GD}} \to \overline{P_D^{GD}}$.

Figure 10 presents a comparison between CA-CFAR detector and GD in terms of the probability of detection as a function of the *INR* when there is one interfering target at $N = 20, 40$; $P_{FA} = 10^{-4}$; and $SNR = 10$ dB. In the GD case, the frequency content of the interfering target is matched with the AF bandwidth. As expected, the detection performance of both detectors deteriorates if the *INR* increases. In Fig. 10, we can see that the GD still has better performance in comparison with CA-CFAR. For example, at $INR = 10$ dB, $SNR = 10$ dB, and $N = 20$, we obtain $P_D^{CA} = 0.3$ and $P_D^{GD} = 0.38$, respectively.

4.2 Ordered Statistic Technique

In the case of the ordered statistic, the stored data in reference cells are rearranged according to increasing numerical order and the *k*th ordered statistic is chosen as the estimated noise power as shown in Fig. 8b. Thus, the estimation of the narrowband noise power takes the following form:

$$
\hat{\sigma}_n^2 = X_{(k)}. \tag{43}
$$

The average probability of false alarm in the case if the GD employs the ordered statistic noise power estimation technique can be derived using the following form:

$$
\overline{P_{FA}^{GD}} = \int_0^{+\infty} P_{FA}^{GD} \, p_{OS}(THR_{GD}^{norm}) d(THR_{GD}^{norm}), \tag{44}
$$

where $THR_{GD}^{norm} = \dfrac{THR_{GD}}{\sigma_n^2}$ is the normalized GD threshold, and $p_{OS}(THR_{GD}^{norm})$ is the normalized GD threshold pdf in the case of ordered statistic noise power estimation technique, which can be presented in the following form [29]:
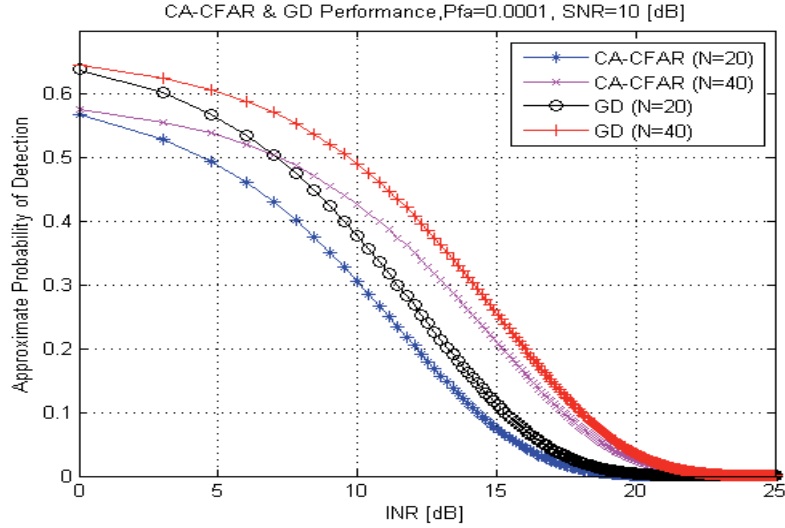
Fig. 10. The approximate probability of detection for GD and CA-CAFR detector as a function of INR.

$$p_{OS}(THR_{GD}^{norm}) = \frac{k}{\gamma_{GD}}\binom{N}{k}\left[\exp\left(-\frac{THR_{GD}^{norm}}{\gamma_{GD}}\right)\right]^{N-k+1}$$

$$\times\left[1-\exp\left(-\frac{THR_{GD}^{norm}}{\gamma_{GD}}\right)\right]^{k-1}. \qquad (45)$$

As follows from (44) and (45), the average probability of false alarm can be determined in the following form:

$$\overline{P_{FA}^{GD}} = \frac{k}{\gamma_{GD}}\binom{N}{k}\int_0^{+\infty}\exp\left(-\frac{THR_{GD}^{norm}}{2}\right)\exp\left[-(N-k+1)\frac{THR_{GD}^{norm}}{\gamma_{GD}}\right]$$

$$\times\left[1-\exp\left(-\frac{THR_{GD}^{norm}}{\gamma_{GD}}\right)\right]^{k-1}d(THR_{GD}^{norm}). \qquad (46)$$

Substituting a new variable $THR_{GD}' = \dfrac{THR_{GD}^{norm}}{\gamma_{GD}}$ in (46), we obtain:

$$\overline{P_{FA}^{GD}} = k\binom{N}{k}\int_0^{+\infty}\exp\left[-\left(\frac{\gamma_{GD}}{2}+N-k+1\right)THR_{GD}'\right]$$

$$\times\left[1-\exp(-THR_{GD}')\right]^{k-1}d(THR_{GD}'). \qquad (47)$$

Using the tabulated integral [28, 3.312.1]:

$$\int_0^{+\infty}\exp(-ax)\left[1-\exp\left(-\frac{x}{b}\right)\right]^{c-1}dx = bB(ab,c), \qquad (48)$$

where a, b, and c are the constants and $B(.,.)$ is the beta function, we obtain the following form:

$$\overline{P_{FA}^{GD}} = k\binom{N}{k}B\left(\frac{\gamma_{GD}}{2}+N-k+1,k\right)$$

$$= k\binom{N}{k}\frac{\Gamma\left(\dfrac{\gamma_{GD}}{2}+N-k+1\right)\Gamma(k)}{\Gamma\left(\dfrac{\gamma_{GD}}{2}+N+1\right)}. \qquad (49)$$

In (48) we use the following notations

$$\begin{cases} a = \dfrac{\gamma_{GD}}{2}+N-k+1; \\ b = 1\,; \\ c = k\,; \\ x = THR_{GD}'\,; \end{cases}$$

The beta function in (49) is expressed using the gamma function $\Gamma(\cdot)$. In the case when γ_{GD}, N, and k are the integers and using $\Gamma(n)=(n-1)!$, (49) can be rewritten as

$$\overline{P_{FA}^{GD}} = k\frac{N!}{k!(n-k)!}\frac{(k-1)!\left(\dfrac{\gamma_{GD}}{2}+N-k\right)!}{\left(\dfrac{\gamma_{GD}}{2}+N\right)!}$$

$$= \frac{N!\left(\dfrac{\gamma_{GD}}{2}+N-k\right)!}{(N-k)!\left(\dfrac{\gamma_{GD}}{2}+N\right)!}. \qquad (50)$$

The average GD probability of false alarm $\overline{P_{FA}^{GD}}$ is presented in Fig. 11 as a function of the threshold scaling factor γ_{GD} when GD employs the ordered statistic noise power estimation technique applying the $k=0.75N$ basis. As we can see from Fig. 11, the GD has a behavior depending on the number of cells N and, as consequence, on the value of k. Figure 11 can be used to determine the GD threshold scaling factor to estimate the specific average probability of false alarm $\overline{P_{FA}^{GD}}$ for a given sliding window configuration.
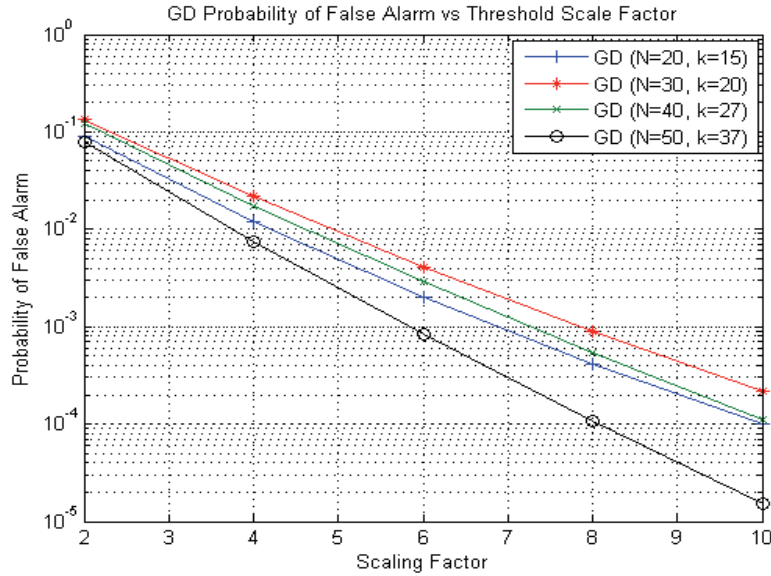
Fig. 11. The GD probability of false alarm as a function of threshold scaling factor in the case of ordered statistic noise power estimation technique.

5.   Simulation Results

5.1   Conditions of Simulation

In practice, the probability of detection P_D is determined as the ratio between the number K_o of the detector output process overshoots with respect to the detection threshold and the total number of observations K [30]:

$$P_D = \frac{K_o}{K} .$$
(51)

Comparison of detection performances between the GD and CFAR detectors based on simulation results is made under the same initial conditions. The probability of false alarm P_{FA} is equal to 10^{-4}. The number of reference cells of the sliding window is $N = 20$ and no guide cells. The number of observations is $K = 1000$. The probability of false censoring P_{FC} in the case of GCML and ACGO-CFAR detectors is equal to 10^{-3}. The selected reference cell in the case of OS-CFAR detector is 15, i.e. $k = 15$. The interfering signals are modeled by the Swerling 2 model of fluctuations [31].

5.2   Discussion of Results

5.2.1. Frequency Content of Interfering Signals is within the Limits of GD PF Bandwidth

In the first scenario (see Fig. 12), there are the subject target and few interfering targets. We assume that the frequency content of interfering signals is within the limits of GD PF bandwidth, which in its turn is matched with the target return signal bandwidth.

Figure 13 demonstrates a comparison between the GD, CA-CFAR detector, and OS-CFAR detector by detec-

tion performance for the following cases:

- there are no interfering targets;
- there is one interfering target;
- there are two interfering targets.

The GD noise power estimation is based on averaging the data in the reference cells of sliding window, as well as for the CA-CFAR detector.
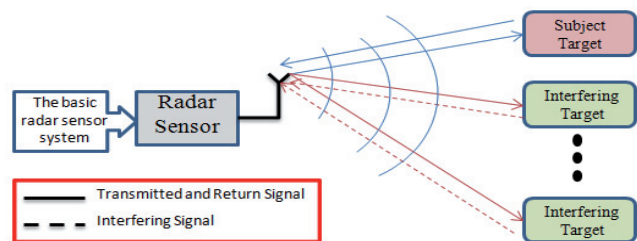
Fig. 12. Scenario 1: the basic radar sensor system is equipped by GD.

As follows from Fig. 13, the GD demonstrates superiority in detection performance for wide range of SNR and for all considered cases. For example, when there is no interference and the probability of detection P_D is equal to 0.6, a superiority of GD in SNR in comparison with, for example, the CA-CFAR detector is for about 2 dB and 2.5 dB in comparison with OS-CFAR detector. For one interfering target when the probability of detection P_D is 0.6, the SNR gain in favor of GD is approximately 7 dB comparing with the CA-CFAR detector and 2.5 dB comparing with the OS-CFAR detector. For two interfering targets, the SNR gain in favor of GD is 3 dB comparing with the OS-CFAR detector at the probability of detection P_D equal to 0.6. In the case of two interfering targets, the CA-CFAR detector performance degradation is severe. The GD presents a great robustness against the interference if the frequency content of interfering signals is matched with

the PF bandwidth, because such interference does not effect on the GD background noise power estimation and, consequently, on the definition of the adaptive GD detection threshold THR_{GD}.

If there are no interfering targets, the CA-CFAR detection performance is better in comparison with OS-CFAR detection performance. If one or two interfering targets are presented, the OS-CFAR detector performance becomes much better in comparison with the CA-CFAR detector performance. As the number N of reference cells of the sliding window is increased, the estimated GD background noise power should be converged to the true value. Thus, the big size of sliding window is usually preferable. In the case of CA-CFAR detector under non-homogenous noise caused by interfering targets, the small number N of reference cells of sliding window allows us to reduce the effects of interfering signals. On the other hand, the CFAR detection losses are decreased when the number of reference cells of sliding window is increased [3]. For small sliding window size, i.e. $N < 20$, the CFAR detection losses can be for about 3 dB at the probability of false alarm P_{FA} equal to 10^{-4} when the probability of detection P_D is 0.9 [3]. The condition $N < 10$ is not acceptable in practice owing to high CFAR detection losses [3]. By this reason we carry out the simulation at $N = 20$.

Figure 14 demonstrates a comparison of detection performance between four detectors, namely, GD, OS-CFAR, GCML, and ACGO-CFAR detectors for three cases: there is no interference, one interfering target, and two interfering targets. The GD presents the better detection performance among these detectors. If there is no interfering target, and when the probability of detection P_D is equal to 0.6, the SNR gain in favor of GD is approximately 2 dB, 2 dB, and 3 dB comparing with the GCML, OS-CFAR, and ACGO-CFAR detectors, respectively. The detection performances of the OS-CFAR and GCML detectors are very close to each other with slightly vantage to GCML one. The ACGO-CFAR detection performance is the worst case among these detectors.

In the case of one interfering target, all detectors demonstrate the robustness against interference with small degradation in the detection performance. We do not include the CA-CFAR detector owing to severe deterioration of the detection performance when there are the interfering signals. As follows from Fig. 14, the GD superiority in SNR is evident. For example, when the probability of detection P_D equals to 0.6, the SNR gain in favor of GD is approximately 2 dB, 2 dB, and 3 dB comparing with the GCML, OS-CFAR, and ACGO-CFAR detectors, respectively. In the case of two interfering targets, at the probability of detection P_D equal to 0.6, the CG achieves for about 4 dB SNR gain in comparison with the ACGO-CFAR detector, 2.5 dB SNR gain comparing with the GCML detector, and 3 dB SNR gain comparing with OS-CFAR detector.

Figure 15 demonstrates the GD, OS-CFAR, GCML, and ACGO-CFAR detection performance when there are five and six interfering targets. All detectors show considerable degradation in the detection performance. For five interfering targets case, at the probability of detection P_D equal to 0.6, the GD achieves 2 dB SNR gain with respect to the GCML and OS-CFAR detectors and approximately 4 dB SNR gain comparing with the ACGO-CFAR detector. For the case of six interfering targets, at the probability of detection P_D equal to 0.6 the GD has superiority in SNR gain for about 2 dB comparing with the GCML detector For the case of six interfering targets, at the probability of detection P_D equal to 0.6 the GD has a superiority in SNR gain for about 2 dB comparing with the GCML detector and 3.5 dB comparing with ACGO-CFAR detector. Additionally, we see that the OS-CFAR detection performance degrades sharply in the case of six interfering targets. OS-CFAR detector demonstrates a good detection performance when the number of interfering targets is not more than five since $N = 20$ and $k = 15$ ($N - k = 5$).

Thus, five interfering targets is a critical case for OS-CFAR detector under condition $N = 20$ and additional interfering target causes a severe degradation in detection
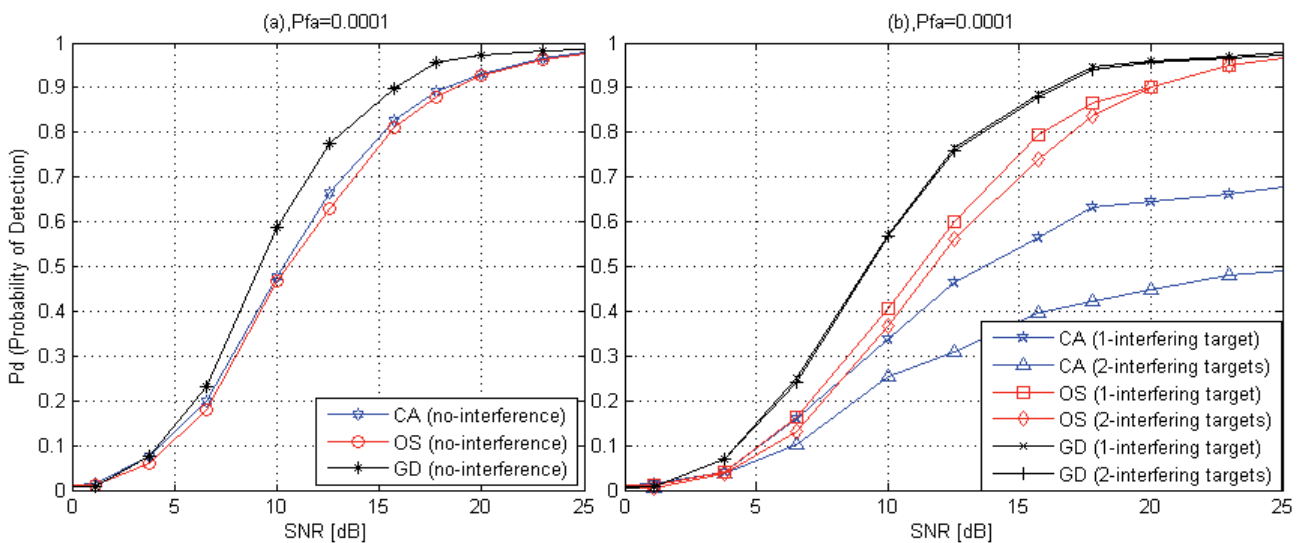
Fig. 13. GD, CA-CFAR, and OS-CFAR detection performance: a) no interference, b) one interfering target and two interfering targets.
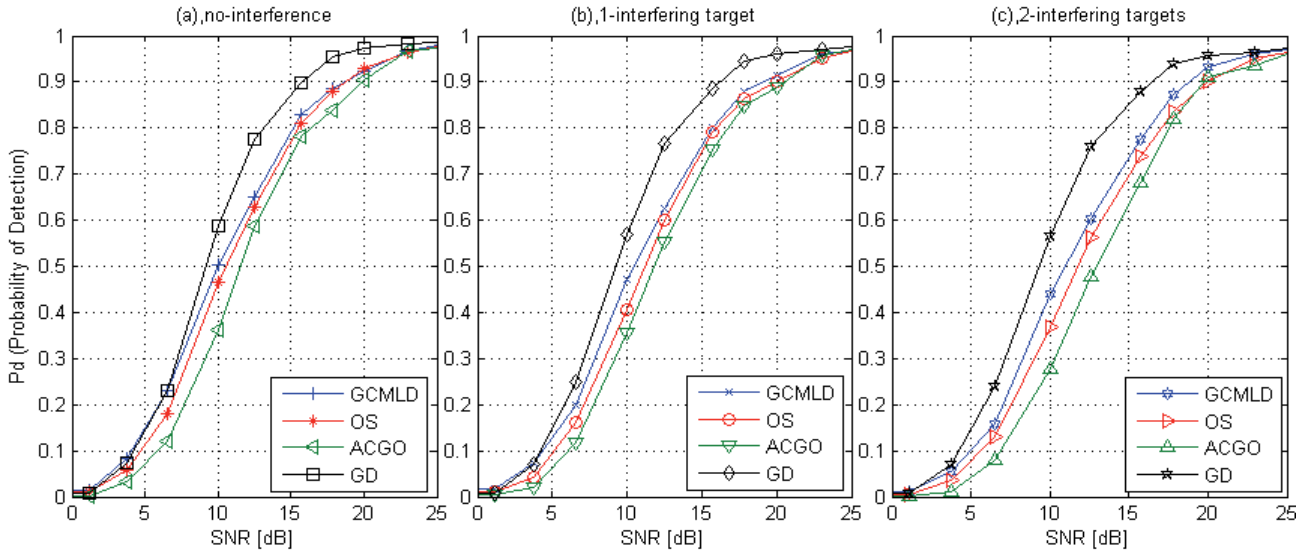
Fig. 14. GD, OS-CFAR, GCML, and ACGO-CFAR detection performance: a) no interference, b) one interfering target, c) two interfering targets.
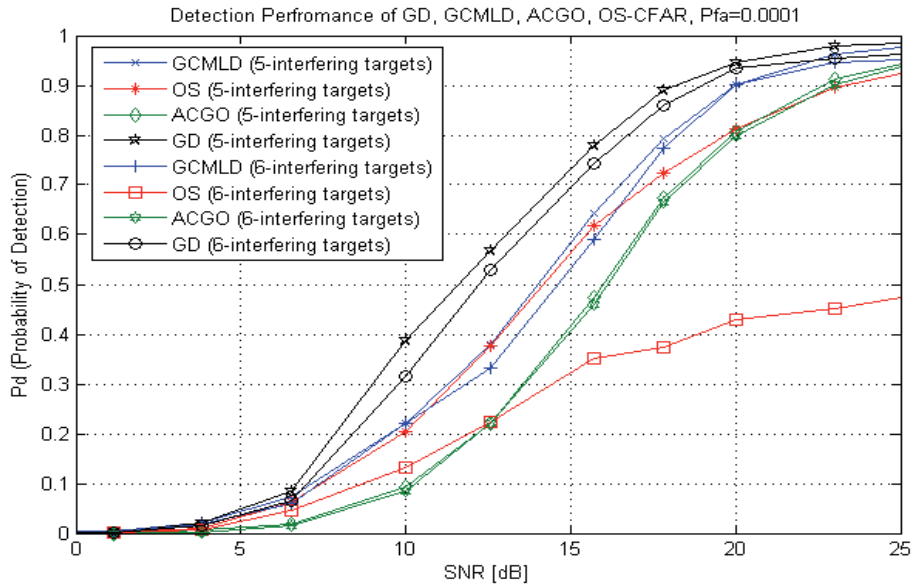
Fig. 15. GD, OS-CFAR, GCML, and ACGO-CFAR detection performance: five interfering targets, and six interfering targets.

performance. This problem for OS-CFAR detector can be solved by increasing the number N of the reference cells of sliding window, for example, $N > 20$. Furthermore, the GD, GCML, and ACGO-CFAR detectors have a reliable detection performance regardless of the number of interfering targets and any prior knowledge about this number.

In general, the GD presents the better detection performance in comparison with the mentioned CFAR detectors and suffers from small detection performance degradation under interfering signals action. In the course of simulation, the number of reference cells N is fixed that allows us to deliver a fair comparison between the detectors and show a difference in the detection performance under the same initial conditions.

5.2.2. Frequency Content of Interfering Signals is both within the Limits of GD PF Bandwidth and GD AF Bandwidth

We consider a special scenario assuming that additionally to the basic radar sensor system there is another radar sensor system with different operation frequency and bandwidth. According to this scenario, the frequency content of interfering signals reflected from the targets after being transmitted by another radar sensor system with operation parameters differing from the parameters of the basic radar sensor system may be within the limits of the GD AF bandwidth and cannot pass through the GD PF. In this case, these interfering signals effect on the noise power estimation procedure and, consequently, on the GD detection performance. This scenario is illustrated in Fig. 16.
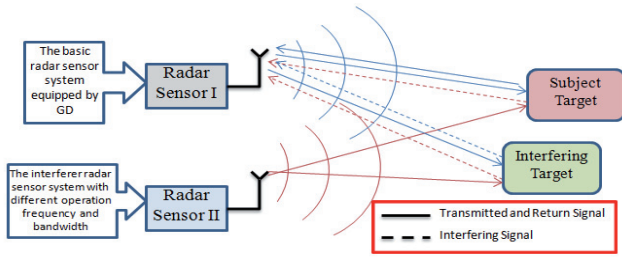
Fig. 16. Scenario 2: there is another radar sensor system with different operation frequency and bandwidth.

Figure 17 demonstrates the detection performance of the GD, CA-CFAR, and OS-CFAR detectors when the GD noise power estimation procedure is based on averaging the data stored in the reference cells of sliding window. The following cases for GD are presented in Fig. 17. In the first case there are one interfering signal the frequency content of which is within the limits of GD PF bandwidth and another interfering signal the frequency content of which is within the limits of GD AF bandwidth. In the second case, there are two interfering signals with the frequency content within the limits of GD PF bandwidth and two interfering signals with the frequency content within the limits of GD AF bandwidth. All the interfering signals with frequency content within the limits of GD AF are generated by another additional radar sensor system. These interfering signals come in at the input of the basic radar sensor system equipped by GD after reflection from the interfering targets In this case, the GD detection performance is deteriorated. For example, at the probability of detection P_D equal to 0.6, the SNR gain is about 3 dB in favor of OS-CFAR in comparison with GD. If there are two interfering targets, we observe a considerable deterioration in the GD detection performance.

In order to eliminate the GD detection performance degradation against the interfering signals, the frequency content of which is within the limits of the GD AF band-width, we can use the noise power estimation procedure similar to the OS-CFAR detector one (Fig. 8b).

Comparison of detection performance between GD and OS-CFAR detector for both cases, namely, a "no" and a "yes" interfering targets is presented in Fig. 18 when the estimation procedure of the GD noise power is similar to the technique used in the case of the OS-CFAR detector (Fig. 8b). When there are the interfering targets, the GD detection performance is evaluated under the same scenario as in Fig. 16 for two cases:

- The first case: there are one interfering signal, the frequency content of which is within the limits of GD PF bandwidth, and another interfering signal, the frequency content of which is within the limits of GD AF bandwidth;

- The second case: there are two interfering signals with the frequency content within the limits of GD PF bandwidth and two interfering signals with the frequency content within the limits of GD AF bandwidth.

The GD demonstrates the better detection performance in both cases. For example, when the probability of detection P_D is 0.6, the SNR gain in favor of the GD is approximately 2 dB and 2.5 dB for one and two interfering targets, respectively, in comparison with the OS-CFAR detector.

6. Conclusions

To define the adaptive detection threshold under implementation of GD in radar sensor systems we apply two background noise power estimation procedures based on the sliding window technique, namely, averaging and ordered statistic processing procedures of data in the reference cells of the sliding window.
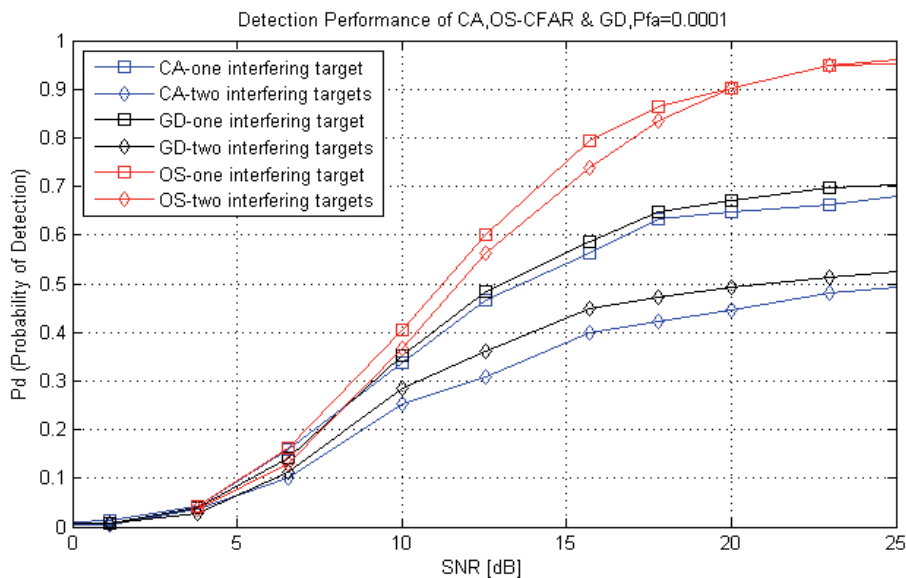
Fig. 17. CA-CFAR, OS-CFAR, and GD detection performance: the frequency content of interfering signals is within the limits of PF and AF bandwidths. The GD background noise power estimation is based on averaging the data in the reference cells of sliding window.
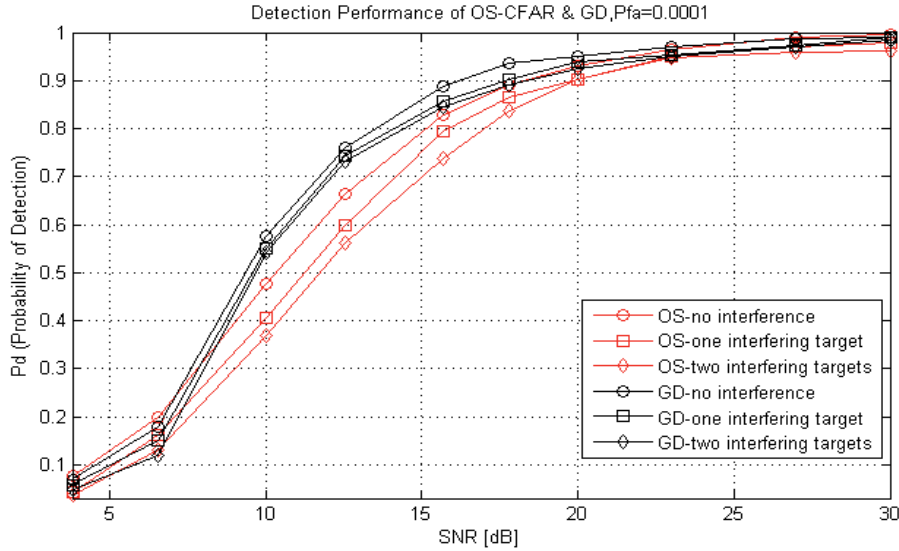
Fig. 18. Comparison of OS-CFAR and GD detection performance: the frequency content of interfering signals is within the limits of PF and AF bandwidths. The GD noise power estimation procedure is similar to the OS-CFAR detector one.

The GD demonstrates the better detection performance in comparison with the mentioned CFAR detectors and achieves a great robustness against the interfering targets. We compare the detection performance of GD and several CFAR detectors, namely, CA-CFAR detector, OS-CFAR detector, GCML detector, and ACGO-CFAR detector. When there is no interfering target and the probability of detection P_D is equal to 0.6, the GD demonstrates the SNR gain of 2 dB, 2.5 dB, 2 dB, and 3 dB in comparison with CA-CFAR, OS-CFAR, GCML, and ACGO-CFAR detectors, respectively. If there is one interfering target and the probability of detection P_D is 0.6, the GD runs up the SNR gain equal to 2.5 dB, 2 dB, and 3 dB in comparison with the OS-CFAR, GCML, and ACGO-CFAR detectors, respectively.

If there are two interfering targets and the probability of detection P_D equals to 0.6, the SNR gains in favor of the GD are 3 dB, 4 dB, and 2.5 dB comparing with OS-CFAR, ACGO-CFAR, and GCML detectors, respectively. In the case of five interfering targets at the probability of detection P_D equal to 0.6, the GD achieves the SNR gain equal to 2 dB, 2 dB, and 4 dB in comparison with OS-CFAR, GCML, and ACGO-CFAR detectors, respectively. For six interfering targets, the SNR gain in favor of the GD is approximately 2 dB comparing with the GCML detector and 3.5 dB SNR gain in comparison with the ACGO-CFAR detector. The OS-CFAR detection performance degrades sharply in the case of six interfering targets owing to that the number of interfering targets is more than $N - k$.

The ordered statistic noise power estimation procedure (Fig. 8b) is employed by GD when the frequency content of the interfering signals reflected from the targets after being transmitted by another radar sensor system with different operation frequency and bandwidth in comparison with the basic radar sensor system is within the limits of the GD AF bandwidth. At the probability of detection P_D

equal to 0.6, comparing with OS-CFAR detector, we see that the GD achieves the SNR gain equal to 2 dB and 2.5 dB for one interfering signal the frequency content of which is within the limits of GD PF bandwidth and one interfering signal the frequency content of which is within the limits of GD AF bandwidth, and for two interfering signals the frequency content of which is within the limits of GD PF bandwidth and two interfering signals the frequency content of which is within the limits of GD AF bandwidth, respectively.

The problem dealing with the interfering signals, the frequency content of which is within the limits of the GD AF bandwidth, leads us to the future research based on employment of interference cancellation approach, for example, beamforming and antenna array with or without direction of arrival estimation with the purpose to eliminate the interference effect on the GD detection performance.

Acknowledgements

References

[1] RICHARDS, M. A. *Fundamentals of Radar Signal Processing.* McGraw-Hill, New York, 2005.

[2] KAY, S. *Fundamentals for Statistical Signal Processing, Vol. II: Detection Theory*. Upper Saddle River (New Jersey): Prentice Hall PTR, 1998.

[3] KAY, S. *Fundamentals for Statistical Signal Processing, Vol. I: Estimation Theory*. Englewood Cliffs (NJ): Prentice Hall, 1993.

[4] KLOTZ, M., ROHLING, H. 24GHz radar sensors for automotive applications. *Journal of Telecommunications and Information Technology*, 2001, vol. 4, p. 11 – 14.

[5] JEONG, S. H., OH, J. N., LEE, K. H. Design of 24 GHz radar with subspace based digital beam forming for ACC stop-and-go system. *ETRI Journal*, 2010, vol. 32, no. 5, p. 827 – 830.

[6] ROHLING, H. OS-CFAR performance in a 77 GHz radar sensor for car application. In *Proceedings of CIE International Conference of Radar*. Beijing (China), Oct. 1996, p. 109 – 114.

[7] LEE, I. B., SHBAT, M. S., YI, J. H., TUZLUKOV, V. P. Signal processing algorithm for blind spot detection using 24 GHz FMCW radar sensor system. In *Proc. of the 11th Asia-Pacific ITS Forum & Exhibition*. Kaohsiung (Taiwan), 2011, (CD).

[8] LEE, I. B., YI, J. H., TUZLUKOV, V. P. 24 GHz FMCW radar systems for blind spot detection system. In *Proceedings of the International Conference of the Korean Society of Automotive Engineers (KSAE)*. Jeju (South Korea), May 2011, p. 1337 – 1342.

[9] YI, J. H., LEE, I. B., SHBAT, M. S., TUZLUKOV, V. P. 24 GHz FMCW radar sensor algorithms for car applications. In *Proceedings of the International Radar Symposium (IRS 2011)*. Leipzig (Germany), Sept. 2011, p. 465 – 470.

[10] FINN, H., JOHNSON, R. Adaptive detection mode with threshold control as a function of spatially sampled clutter-level estimates. *RCA Review*, 1968, vol. 29, no. 3, p. 414 – 464.

[11] ROHLING, H. Radar CFAR thresholding in clutter and multiple target situations. *IEEE Transactions on Aerospace and Electronic Systems*, 1983, vol. 19, no. 4, p. 608 – 621.

[12] GANDHI, P., KASSAM, S. Analysis of CFAR processors in nonhomogeneous background. *IEEE Transactions on Aerospace and Electronic Systems*, 1988, vol. 24, no. 4, p. 427 – 445.

[13] KHALIGHI, M. A., BASTANI, M. H. Adaptive CFAR processor for nonhomogeneous environments. *IEEE Transactions on Aerospace and Electronic Systems,* 2000, vol. 36, no. 3, p. 889 – 897.

[14] MAGAZ, B., BELOUCHRANI, A., HAMADOUCHE, M. Automatic threshold selection in OS-CFAR radar detection using information theoretic criteria. *Progress in Electromagnetics Research B*, 2011, vol. 30, p. 157 – 175.

[15] HIMONAS, S. D., BARKAT, M. A robust radar CFAR detector for multiple target situations. In *Proceedings of IEEE National Radar Conference*. Dallas (USA), March 1989, p. 85 – 90.

[16] HIMONAS, S. D. Adaptive censor greatest-of CFAR detection. *IEE Proceedings-F, Radar and Signal Processing*, 1992, vol. 139, no. 3, p. 247 – 255.

[17] TUZLUKOV, V. P. A new approach to signal detection theory. *Digital Signal Processing: A Review Journal*, 1998, vol. 8 no. 3, p. 166 – 184.

[18] TUZLUKOV, V. P. *Signal Detection Theory*. Springer-Verlag, Boston, 2001.

[19] SHBAT, M. S., TUZLUKOV, V. P. Generalized approach to signal processing in noise for closing vehicle detection application using FMCW radar sensor system. In *Proceedings of the International Radar Symposium (IRS 2011)*. Leipzig (Germany), Sept. 2011, p. 459 – 464.

[20] SHBAT, M. S., TUZLUKOV, V. P. Signal processing in automotive controller area network based on radar sensors. In *Proceedings of the 11th International Conference on Control, Automation, and Systems (ICCAS 2011)*, Gyeonggi-do (South Korea), Oct. 2011, p. 616 – 620.

[21] SHBAT, M. S., TUZLUKOV, V. P. Generalized detector with adaptive detection threshold for radar sensors. In *Proceedings of the International Radar Symposium (IRS 2012)*. Warsaw (Poland), May 2012, p. 91 – 94.

[22] Draft International Standard ISO/DIS 17387, Intelligent transportation systems - lane change decision aid systems - performance requirements and test procedures, *International Organization for Standardization*, 2006.

[23] SHBAT, M. S., TUZLUKOV, V. P. CFAR detectors employed by radar sensor systems. In *Proceedings of the 12th International Conference on Control, Automation, and Systems (ICCAS 2012)*. Jeju (South Korea), Oct. 2012, p. 518 – 522.

[24] MAXIMOV, M. Joint correlation of fluctuative noise at outputs of frequency filters. *Radio Eng*., 1956, no. 9, p. 28 – 38.

[25] CHERNYAK, Y. Joint correlation of noise voltage at outputs of amplifiers with non-overlapping responses. *Radio Phys. and Elec.*, 1960, no. 4, p. 551 – 561.

[26] TUZLUKOV, V. P. *Signal Processing Noise*. Boca Raton, London, New York, Washington D.C.: CRC Press, Taylor & Francis Group, 2002.

[27] TUZLUKOV, V. P. *Signal Processing in Radar Systems*. Boca Raton, London, New York, Washington D.C: CRC Press, Taylor & Francis Group, 2012.

[28] GRADSHTEYN, I. S., RYZHIK, I. M. *Table of Integrals, Series, and Products*. 7th ed., Elsevier, Academic Press, 2007.

[29] LEVANON, N. *Radar Principles*. New York: J. Wiley & Sons (Interscience Div.), 1988.

[30] MAHAFZA, B. R., ELSHERBENI, A. Z. *Matlab Simulation for Radar Systems Design*. Chapman & Hall/CRC Press LLC, 2004.

[31] SWERLING, P. Probability of detection for fluctuating targets. *IRE Transactions on Information Theory*, 1960, vol. IT-6, p. 269 to 308.